JOURNAL OF MATERIALS SCIENCE **34** (1999) 5871–5878

Viscoplastic modeling of ABS material under high-strain-rate uniaxial elongational deformation

S. WANG*, A. MAKINOUCHI
Materials Fabrication Laboratory, The Institute of Physical and Chemical Research, 2-1 Hirozawa, Wako-shi, Saitama, 351-0198, Japan
E-mail: swang@postman.riken.go.jp

M. OKAMOTO, T. KOTAKA
Polymeric Materials Engineering, Toyota Technological Institute, 2-12-1 Hisakata, Tempaku, Nagoya, 468, Japan

T. NAKAGAWA
Institute of Industrial Science of the University of Tokyo, 7-22-1 Roppongi, Minato, Tokyo, 106, Japan

Uniaxial tensile tests were performed on the newest type of Meissner rheometer with an ABS (acrylonitrile-butadiene-styrene) material. Tests were conducted for constant strain rates varying from 0.01 to 1 (1/s), at the temperatures ranging from 150 to 200 °C. Based on the experimental data, a new model was proposed, in which, strain hardening, strain rate sensitivity, temperature changes and the variation in the hardening index could be taken into consideration. In this new model, a new parameter, w, was introduced, which represents the variation in the hardening index. The proposed model can approximate the experimental data of the uniaxial tensile test quite well. Two existing models were also employed to approximate the material behavior, however, both of them exhibited the poor accuracy. Finally, a simple stretch deformation was simulated employing the three different models, and the differences in the final thickness and shape were confirmed.

1. Introduction

In the last few years, research in the simulation of thermoforming and blow molding processes has been actively conducted. One of the key issues in this research field is to develop an accurate material model. Various constitutive equations have been employed to simulate the processes, including hyperelastic [1, 2], viscoelastic [3, 4] and viscoplastic [5–7] models. Since high speed elongational deformation is the dominant deformation mode in the thermoforming and blow molding processes, a suitable constitutive equation should be established by investigating the elongational deformation behavior of the material at a high strain rate. However, little research has been performed under such conditions. In particular, there have been almost no detailed studies on the combined effects of strain hardening, strain rate sensitivity, and temperature changes under the conditions at which thermoforming and blow molding is conducted. Therefore, the aim of this work is to perform suitable material tests, with the strain, strain rate and temperature ranges setting to be close to the real processes, and to propose an accurate and simple material model to describe the material's elongational deformation behavior.

On choosing a suitable test machine, we found that the newest type of Meissner elongational rheometer [8] is more advantageous for performing such a test than the conventional machines, with which the relations between the true stress and the true strain can be obtained under constant true strain rates at different temperatures. Using this rheometer, we conducted the tensile tests for the ABS material under the conditions at which thermoforming is conducted. Based on the test data, a new accurate material model is proposed, in which the flow stress is represented as a function of strain hardening, strain rate sensitivity and temperature. In order to clarify the improvement of the new model, comparison of the precision with the two existing models was also performed. Finally, a simple stretch deformation was simulated employing the three different models, and the differences in the final thickness and shape were confirmed.

2. Experimental instrument

The uniaxial tensile test has been widely used to obtain mechanical properties of polymers. However, a conventional tensile test machine cannot provide sufficient data for simulation of the thermoforming process, which is

* Author to whom all correspondence should be addressed.

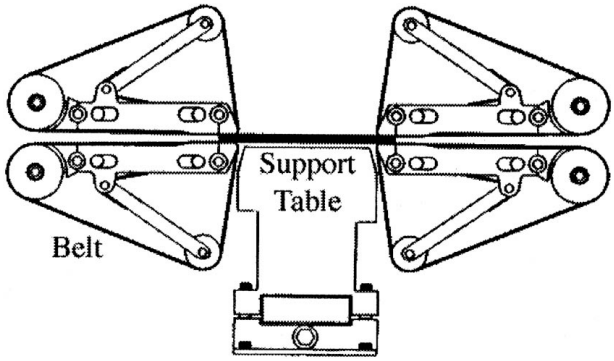

Figure 1 Kernel part of the newest type of Meissner rheometer.

performed at high temperature near the melting point and under a high strain rate (more than 1 (1/s)). This is mainly due to the following three reasons. First, when the temperature is near the melting point, the polymer is susceptible to the clamping force, and the material in the clamping zone can even be squeezed or broken before any stretching is conducted. Second, most of the conventional testing machines operate with a constant increase of the specimen length with time, and the true strain rate changes with the stretching. Therefore, it is difficult to evaluate the strain rate effect correctly. Third, the investigation of polymer's behavior at high strain rate which is a very important characteristic of the thermoforming process is quite difficult with a conventional testing machine. These problems can be overcome by using the newest type of Meissner elongational rheometer equipped with a revised rotary clamp. Fig. 1 shows the kernel part of this rheometer [8]. Each clamp has an upper and a lower belt fixture made of titanium. These fixtures are equipped with conveyor belts made of thin metal bands. The belt has a rough surface formed by deep drawing. This roughness causes perfect sticking of the polymer specimen to the metal belt and leads to an excellent transfer of the velocity from the belt to the specimen. After inserting a polymer specimen into the rheometer, the specimen between the two clamps is supported by a cushion of inert gas that is provided by pressing a gas stream through a metal frit located on top of the specimen support table. The adequate, constant gas pressure can be properly adjusted to ensure a proper support of the specimen without blowing it away or letting it stick to the surface of the frit. The left and right rotary clamps have a fixed distance between them and rotate in the opposite directions. As a result, the specimen is transported out of the zone such that the material located between the rotary clamps is elongated homogeneously, and thus if the speed of rotation of the clamps is kept constant, the true strain rate can be constant. The relations between the true stress and the true strain can be measured for the constant true strain rates ranging from 0.001 to 1 (1/s) at the different temperatures. The maximum true strain is 7 and the temperature can be precisely controlled up to 300 °C (±0.2 °C).

To prepare the isotropic specimens, a hot press is used, and the well-dried pellet is formed into flat sheets of 1 mm thickness. After cooling, the flat sheets are cut into strips with the dimensions of 20 × 60 × 1 mm.

Assuming the deformation of the specimen is homogenous, tensile stress $\sigma(t)$ at time t can be given by:

$$\sigma(t) = F(t)/A(t) \tag{1}$$

Here, $F(t)$ is tensile force and $A(t)$ is the area of the cross section of the polymer specimen at time t.

For a constant tensile true strain rate $\dot{\varepsilon}$, we can simply find the relation between $A(t)$ and the initial area of cross section A_0, assuming that the polymer keeps constant volume during deformation:

$$A(t) = A_0 \exp(-\dot{\varepsilon}t) \tag{2}$$

Therefore the tensile true stress $\sigma(t)$ can be given as:

$$\sigma(t) = F(t) \exp(\dot{\varepsilon}t)/A_0 \tag{3}$$

Because the deformation of the specimen can be affected by the preparation of the sheet and sometimes is not homogeneous due to the improper setting of the specimen between the clamps, it is necessary to confirm the deformed shape of the specimen. This can be monitored with a video camera system through a window inlaid in the upper wall of the oven. The deformation images of ABS material taken by the video camera under the constant strain rate of 0.1 (1/s) at the temperature of 150 °C, are shown in Fig. 2, in which homogenous extension can be observed.

3. Experimental results

The tensile tests were conducted for the ABS (acrylonitrile-butadiene-styrene) material SE-100 provided by Denki Kagaku Kogyo Co. Ltd., at the strain rates ranging from 0.01 to 1 (1/s) and the temperatures varying from 150 to 200 °C, which are the expected deformation ranges in the actual thermoforming process. Because the qualitative tendencies of the strain and strain rate effects on the stress are similar at different temperatures, the results obtained at 170 °C are analyzed as an example. Fig. 3 shows the true stress σ vs true strain ε relations obtained under different constant strain rates for 170 °C. Since the true stress σ increases with the true strain ε almost linearly in a log-log plot, it might be reasonable to approximate the strain hardening relation by following equation:

$$\sigma = k\varepsilon^n \tag{4}$$

The slopes of the straight lines (n in Equation 4) shown in Fig. 3 and the approximation correlation coefficients are listed in Table I. Because the average value of the correlation coefficients is equal to 0.99642, which is quite close to 1, we can say that the test data under a constant strain rate can be properly approximated by Equation 4. Table I shows that when the strain rate increases from 0.01 to 1, the slope n increases from 0.381 to 0.907.

TABLE I Slopes and correlation coefficients for constant strain rates

Strain rate (1/s)	0.01	0.05	0.1	0.5	1	Average
Slope	0.381	0.575	0.669	0.823	0.907	0.671
Correlation	0.99495	0.9961	0.9942	0.99702	0.99981	0.99642

Figure 2 Images of sample deformation in four selected steps at strain rate of 0.1 (1/s), and temperature of 150 °C. Homogenous deformation can be observed.

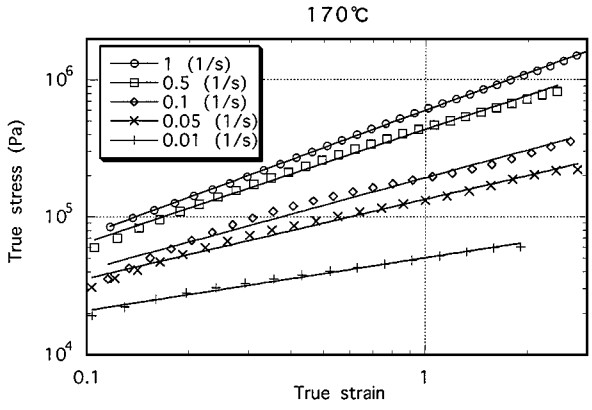

Figure 3 The log-log true stress-true strain relations at 170 °C. Points are the experimental data, and lines are the approximation results of the least square method.

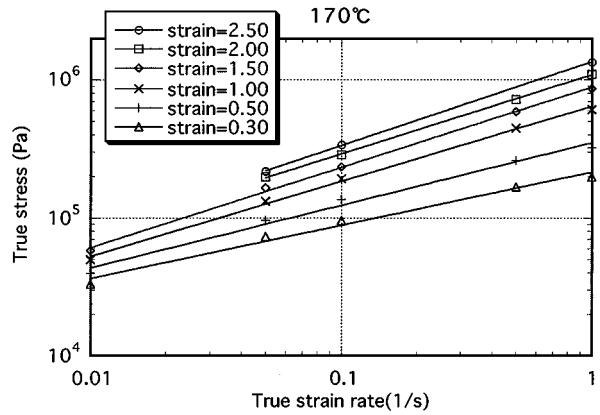

Figure 4 The log-log true stress-true strain rate relations at 170 °C. Points are the experimental data, and lines are the approximation results of the least square method.

In order to evaluate the effect of the strain rate $\dot{\varepsilon}$ on the stress σ, the true stress σ vs true strain rate $\dot{\varepsilon}$ relations at constant strains $\dot{\varepsilon}$ are plotted in Fig. 4, in which the same data shown in Fig. 3 are utilized. Again, applying the least square method to the data under constant strains, we can get the slopes and the correlation coefficients of the approximation lines, whose values are shown in Table II. The measured σ vs $\dot{\varepsilon}$ relation at a constant strain can be expressed by following equation:

$$\sigma = k\dot{\varepsilon}^{\mathrm{m}} \tag{5}$$

Fig. 5 shows the σ vs ε relations for the constant strain rate of 0.1 (1/s) at different temperatures, where strain hardening can be observed at all the temperatures. The least square approximation results are shown in Table III. It can be seen that with increasing temperature, the slope n becomes smaller gradually, and from the correlation coefficients, it can be also seen that Equation 4 provides quite good approximation for test data under a constant strain rate at different temperatures.

4. New model

Based on the above experimental results, efforts were made to create an accurate and simple material model

TABLE II Slopes and correlation coefficients for constant strains

Strain	0.3	0.5	1	1.5	2	2.5	Average
Slope	0.385	0.454	0.544	0.581	0.574	0.608	0.524
Correlation	0.9932	0.99472	0.99868	0.99977	0.99983	0.99999	0.9977

TABLE III Slopes and correlation coefficients at different temperatures

Temperature (°C)	150	170	190	200	Average
Slope	0.931	0.669	0.392	0.375	0.592
Correlation	0.99926	0.9942	0.99202	0.97126	0.98919

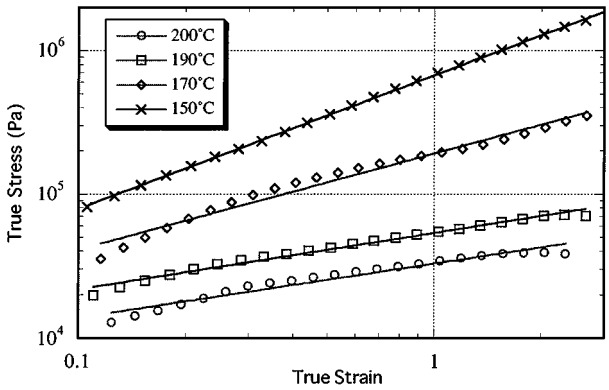

Figure 5 The log-log true stress-true strain relations at different temperature. Points are the experimental data, and lines are the approximation results of the least square method.

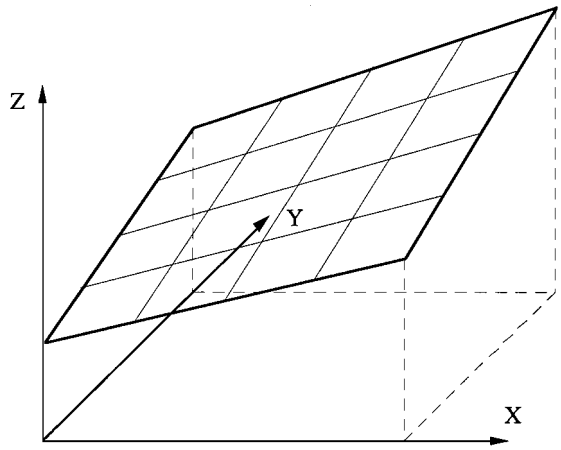

Figure 6 Schematic view of the 3D data distribution at a constant temperature.

for ABS material valid in all the strain, strain rate and temperature ranges covered in the experiment.

When we plot all the experimental data shown in Fig. 3 into (x, y, z) space, with $x = \log \varepsilon$, $y = \log \dot{\varepsilon}$, $z = \log \sigma$, the data constructs a surface which is shown qualitatively in Fig. 6 and can be approximated by the following equation:

$$z = a + bx + cy + dxy \tag{6}$$

that is:

$$\log \sigma = \log k + n' \log \varepsilon + m' \log \dot{\varepsilon} + w \log \varepsilon \log \dot{\varepsilon} \tag{7}$$

Equation 7 describes a bilinear surface, whose characteristic is that the intersection of the surface with a plane normal to a coordinate axis x or y is a straight line, which represents the $\log \sigma$-$\log \dot{\varepsilon}$ line in Fig. 4 or $\log \sigma$-$\log \varepsilon$ line in Fig. 3. The slopes of lines are different from place to place.

Rewriting Equation (7) into an exponential form, we obtain:

$$\sigma = k\varepsilon^{n'} \dot{\varepsilon}^{m' + w \log \varepsilon} \tag{8}$$

where n' is the slope of the $\log \sigma$-$\log \varepsilon$ relation at $\dot{\varepsilon} = 1$, and m' is the slope of $\log \sigma$-$\log \dot{\varepsilon}$ relation at $\varepsilon = 1$, and w can be given as:

$$w = \frac{(\partial \log \sigma / \partial \log \varepsilon)_{\dot{\varepsilon}=c} - n'}{\log c} \quad (c \neq 1) \tag{9}$$

where $(\partial \log \sigma / \partial \log \varepsilon)_{\dot{\varepsilon}=c}$ is the slope of the $\log \sigma$-$\log \varepsilon$ relation at any constant strain rate c except 1, which is obtained from the experiment data. Parameter w represents the variation of the slope.

The strain hardening index n and strain rate sensitivity index m, in Equations 4 and 5, always change according to:

$$n = \left.\frac{\partial \log \sigma}{\partial \log \varepsilon}\right|_{\dot{\varepsilon}=\text{const}} = n' + w \log \dot{\varepsilon} \tag{10}$$

$$m = \left.\frac{\partial \log \sigma}{\partial \log \dot{\varepsilon}}\right|_{\varepsilon=\text{const}} = m' + w \log \varepsilon \tag{11}$$

Equations 10 and 11 reveal that the strain hardening index n is affected by strain rate, while the strain rate sensitivity index m is affected by strain.

Following the above procedures, the material parameters of ABS material at 170 °C are determined:

$$n' = 0.907, \quad m' = 0.544, \quad w = 0.26,$$

$$k = 6.543 \times 10^5$$

All the experimental data at 170 °C can thus be approximated using Equation 8 with the above constants. In order to validate this approximation, Equation (8) and the experimental data at constant $\dot{\varepsilon}$ and ε are plotted in Figs 7 and 8. They clearly correspond to each other quite well. Although the above discussion is made at constant temperature of 170 °C, the data distribution at different temperatures basically shows the same tendency. Therefore we may assume that Equation 8 can be applicable for different temperatures. Thus the surfaces illustrated in Fig. 6 for 170 °C, is reconstructed for different temperatures, as shown in Fig. 9. Here, it is obvious that the constants k, n', m' and w in Equation 8 are functions of temperature, and then we determine k-T, n'-T, m'-T and w-T by obtaining constant values at different temperatures using Equations 9, 10 and 11.

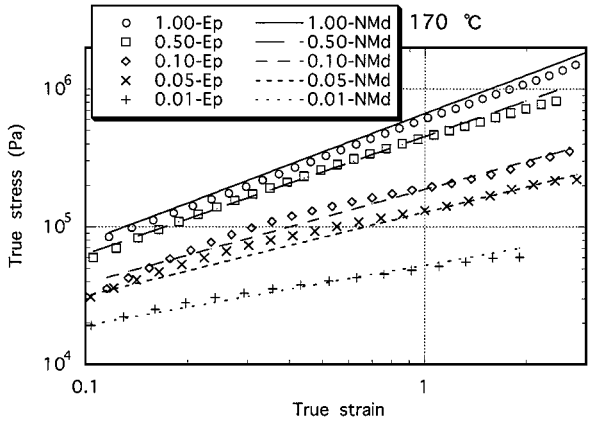

Figure 7 The log-log true stress-true strain relations predicted using new model. Points are the experimental data, and lines are the predicted results of the new model.

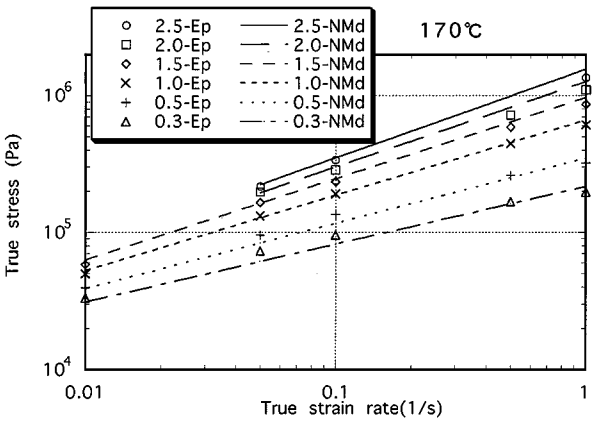

Figure 8 The log-log true stress-true strain rate relations predicted using new model. Points are the experimental data, and lines are the predicted results of the new model.

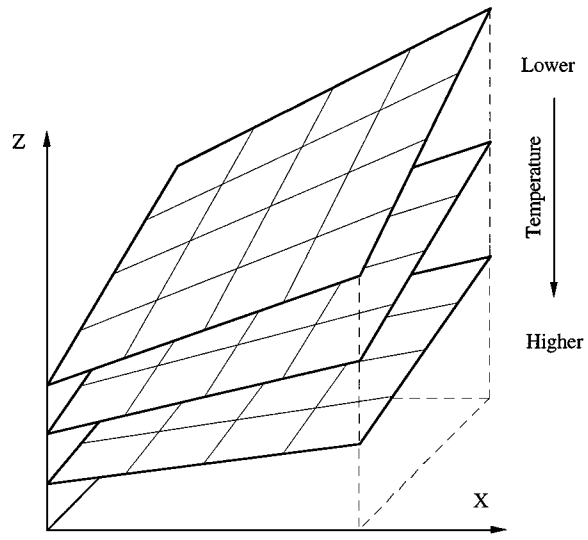

Figure 9 Schematic view of the 3D data distribution at different temperatures.

k decreases exponentially with an increase in temperature, which appears to be a linear relation in a log-log plot as shown in Fig. 10. Relations n'-T, m'-T and w-T are shown in Fig. 11, in which, n' decreases linearly, while m' increases linearly with an increase in temperature. These changes indicate that, as the temperature increases, the strain hardening decreases, and the strain rate sensitivity increases. The same figure also shows

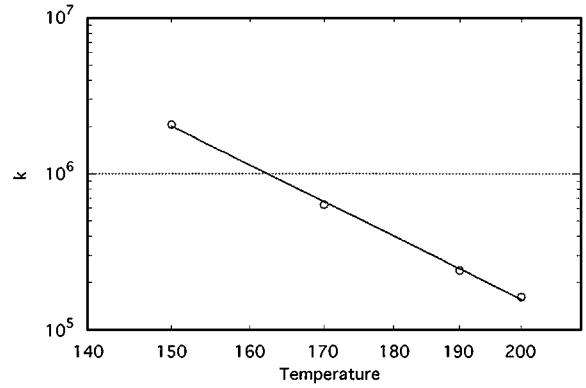

Figure 10 k-T relation. Points are the experimental data, and line is the approximation result of the least square method.

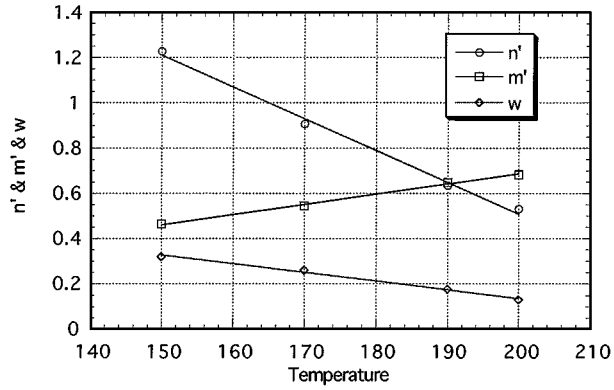

Figure 11 n'-T, m'-T, w-T relations of new model. Points are the experimental data, and lines are the approximation results of the least square method.

that w decreases with an increase in temperature, which reveals that the variation of the slope decreases with increasing temperature.

Except for k-T, which can be best fitted by an exponential relation, all the variables can be best described by the linear relations:

$$k = a_1 T^{b_1}, \quad n' = a_2 + b_2 T, \quad m' = a_3 + b_3 T, \quad w = a_4 + b_4 T \tag{12}$$

For the tested temperature range, the coefficients are $a_1 = 4.2456 \times 10^{25}$, $a_2 = 3.3183$, $a_3 = -0.21649$, $a_4 = 0.89966$, $b_1 = -8.8803$, $b_2 = -0.014049$, $b_3 = 0.0045101$, and $b_4 = -0.00382$.

5. Discussion

5.1. Existing models

In order to clarify the improvement achieved using the above new model, approximations of the experimental data are also conducted with the two existing models for comparison.

a) Model 1. First, we examine the performance of the following well-known non-Newtonian creeping material model, which can be also obtained using the new model with $n' = 0$ and $w = 0$:

$$\sigma = k\dot{\varepsilon}^m \tag{13}$$

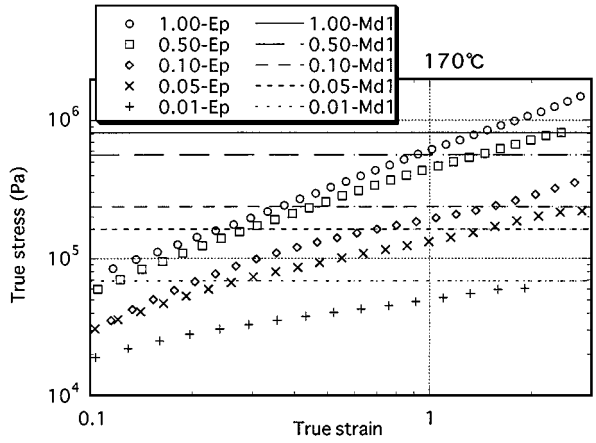

Figure 12 The log-log true stress-true strain relations predicted using model 1. Points are the experimental data, and lines are the predicted results of model 1.

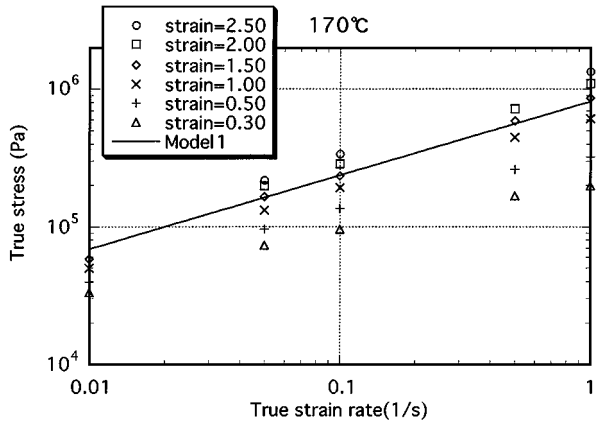

Figure 13 The log-log true stress-true strain rate relation predicted using model 1. Points are the experimental data, and the line is the predicted results of model 1.

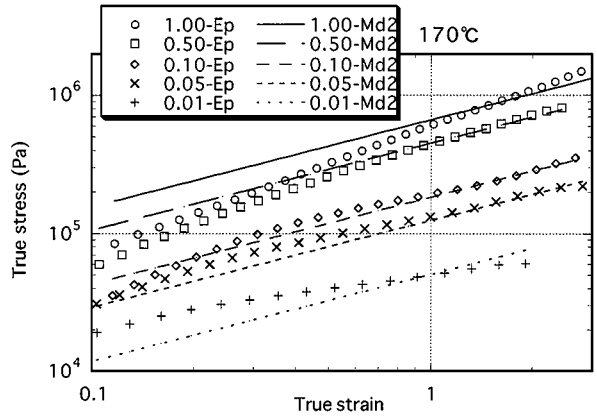

Figure 14 The log-log true stress-true strain relations predicted using model 2. Points are the experimental data, and lines are the predicted results of model 2.

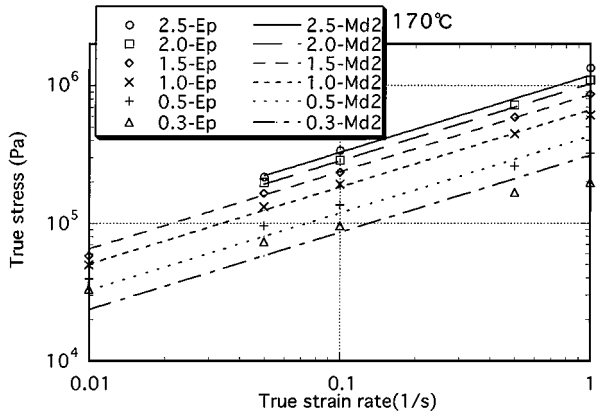

Figure 15 The log-log true stress-true strain rate relations predicted using model 2. Points are the experimental data, and lines are the predicted results of model 2.

where, k and m are the constants. m is given by the average value of the slopes shown in Table II, and k is equal to the stress at $\dot{\varepsilon} = 1$. However, from Fig. 4, we know that at $\dot{\varepsilon} = 1$ the stress values are different at different strains, thus we simply take the average value of them, i.e., $k = 8.124 \times 10^5$.

Substituting the constants $m = 0.671$ and $k = 8.124 \times 10^5$ to Equation 13, and plotting it together with the experimental data, we obtain Figs 12 and 13. Since the strain hardening is not considered in Equation 13, in Fig. 12, the lines predicted by Equation 13 are all parallel to the strain axis. In Fig. 13, the predicted lines become a single line passing through a group of experimental data.

b) Model 2. The following model has been often used to combine the effects of strain rate and strain hardening, which can be also obtained using the new model with $w = 0$:

$$\sigma = k\varepsilon^n \dot{\varepsilon}^m \tag{14}$$

where k, n and m are all constants, and k is equal to the stress values when $\varepsilon = 1$ and $\dot{\varepsilon} = 1$, i.e., $k = 6.543 \times 10^5$. n and m are the strain hardening and strain rate sensitivity indexes, which can be determined by the values in Tables I and II. Although the index values in Tables I and II keep changing, using this model, we have to assume a constant value. Here we take the average values of $n = 0.671$ and $m = 0.524$. Plotting Equation 14 together with the experimental data, we obtain the results as shown in Figs 14 and 15.

Compared with model 1, since strain hardening is considered in model 2, the prediction of model 2 is closer to the experimental data. However, since the predicted lines have a constant slope both in Figs 14 and 15, this model could not reflect the successive changing of the slopes of the experimental data. Table I shows that the slopes change from 0.3–0.9 for the tested strain rate range, this variation should not be neglected in the material model.

In the case of model 2, k-T is the same as that in model 3 and is given in Fig. 10. m-T and n-T are shown in Fig. 16. These relations can be modeled as:

$$k = a_1 T^{b_1}, \quad n = a_2 + b_2 T, \quad m = a_3 + b_3 T. \tag{15}$$

where the constants are

$$a_1 = 4.2456 \times 10^{25}, \qquad a_2 = 1.8507,$$
$$a_3 = -0.08735, \qquad b_1 = -8.88030,$$
$$b_2 = -0.0071782, \quad \text{and} \quad b_3 = 0.0038059.$$

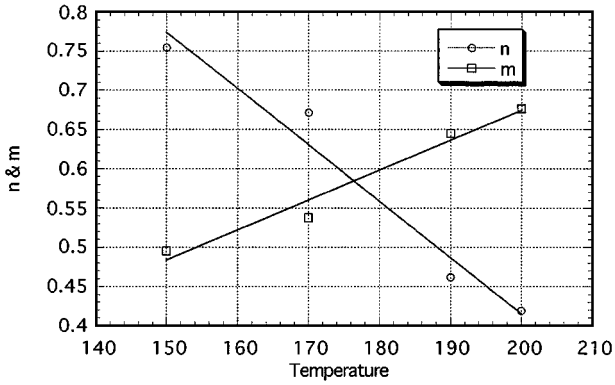

Figure 16 n-T, m-T relations for model 2. Points are the experimental data, and lines are the approximation results of the least square method.

A similar material model, which considered the stress as a function of strain and strain rate, has been proposed by G'Sell and Jonas [9], based on the uniaxial tensile test conducted at room temperature for HDPE and PVC. However, as stated in G'Sell *et al.* [10], in their model, the strain hardening coefficient is independent of the strain rate, and the strain rate sensitivity coefficient is independent of the strain, which are different from the model proposed in this paper.

5.2. FEM simulation

The above three models can all be generalized into 3D deformation cases in terms of equivalent stress $\bar{\sigma}$, equivalent strain $\bar{\varepsilon}$, and equivalent strain rate $\dot{\bar{\varepsilon}}$, e.g., Equation 8 becomes:

$$\bar{\sigma} = k\bar{\varepsilon}^{n'}\dot{\bar{\varepsilon}}^{m'+w\log\bar{\varepsilon}} \tag{16}$$

where $\bar{\sigma} = \sqrt{3/2\sigma'_{ij}\sigma'_{ij}}$, $\dot{\bar{\varepsilon}} = \sqrt{2/3\dot{\varepsilon}_{ij}\dot{\varepsilon}_{ij}}$, $\bar{\varepsilon} = \int_0^t \dot{\bar{\varepsilon}}\,dt$

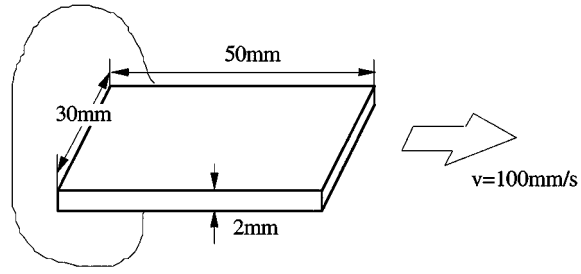

Figure 17 Schematic view of the simulation model.

The viscoplastic constitutive equation is obtained by substituting Equation 16 to the following Levy-Mises flow rule:

$$\sigma'_{ij} = \frac{2\bar{\sigma}}{3\dot{\bar{\varepsilon}}}\dot{\varepsilon}_{ij} \tag{17}$$

Implementing all three models into the viscoplastic FEM code developed by authors, we simulated the stretching tests, and evaluated the differences in the final thickness and shape qualitatively. For the details of FEM formulation refer to [6, 7].

The dimensions of the specimen are $50 \times 30 \times 2$ mm, and one end of the specimen is fixed, while the other is stretched in the longitudinal direction, with the displacement fixed in the transverse direction at both ends (Fig. 17). The comparison is conducted when the specimen length becomes three times of its initial length.

The initial temperature distribution is set artificially. As shown in Fig. 18, the temperature decreases linearly from 160 °C at the middle point to 150 °C at two ends. The deformation is assumed to be conducted under a heat insulation condition due to the high speed process. Fig. 19 shows the thickness distribution obtained using

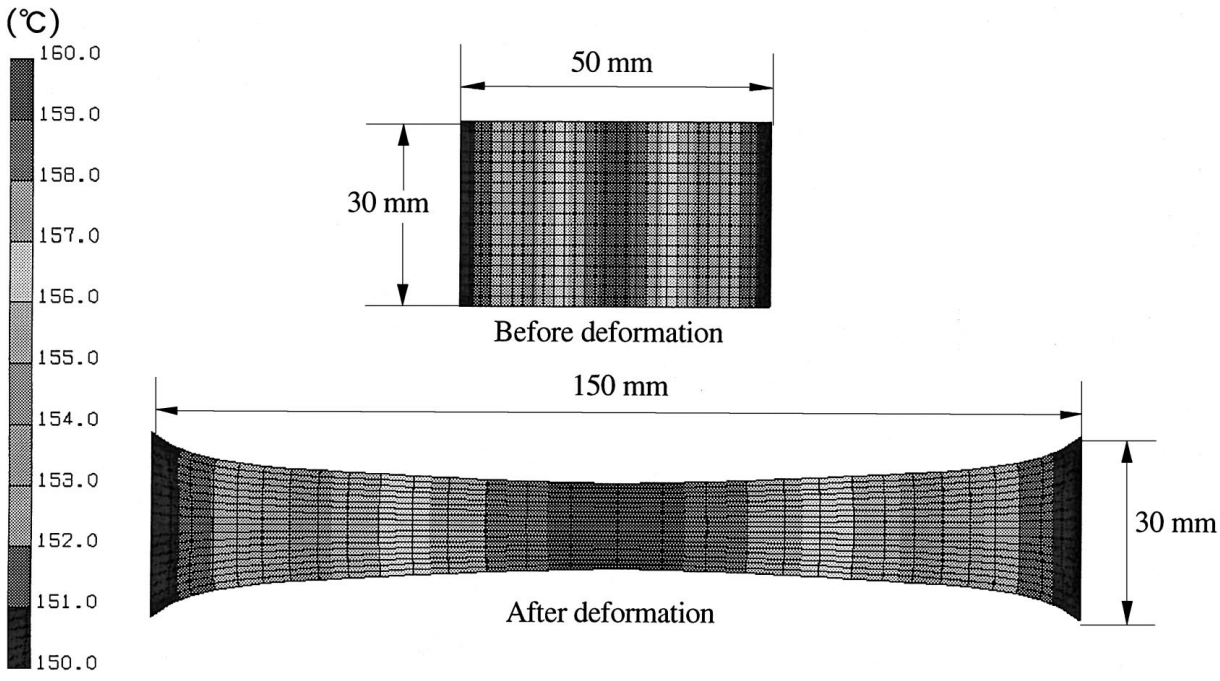

Figure 18 The initial temperature distribution and the temperature distribution when comparison of thickness between models conducted. The temperature decreases linearly from 160 °C at the middle point to 150 °C at two ends, and the deformation is assumed to occur under a heat insulation condition due to the high speed of the process.

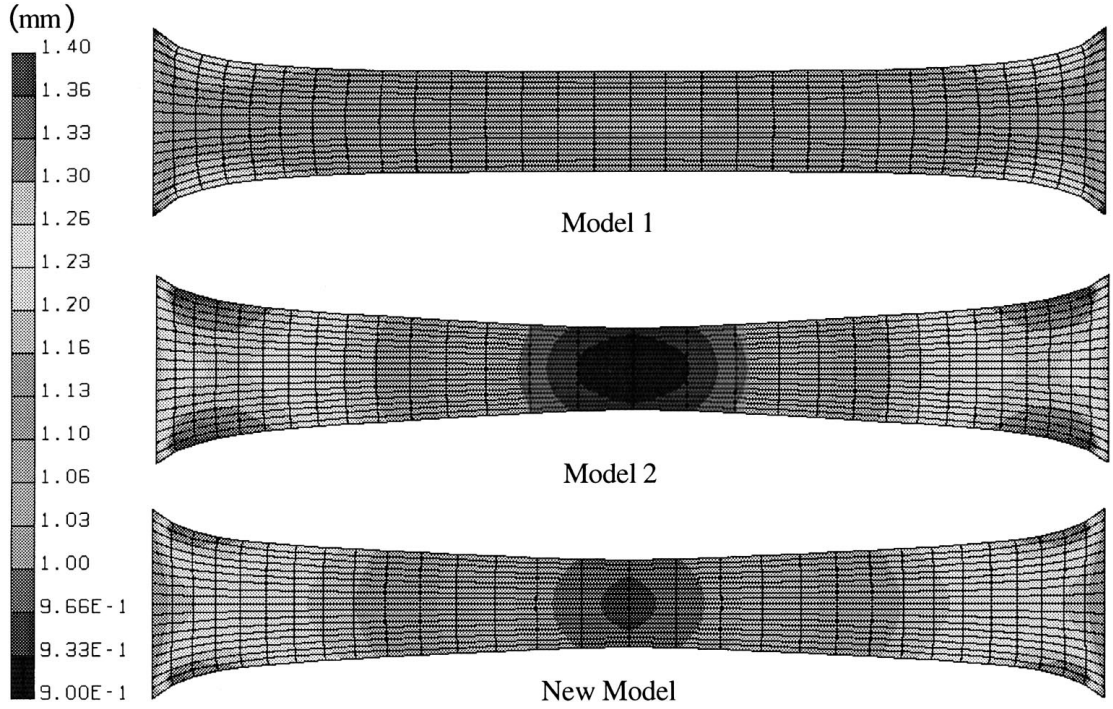

Figure 19 Final thickness distribution obtained using the three models.

the three models. Since the temperature effect is not considered in model 1, the specimen calculated using model 1 is simply uniformly stretched. On the other hand, because the temperature effect is considered in both model 2 and the new model, strain localization is observed in the middle part of the specimen, where the temperature is higher than the surrounding area. However, the strain localization calculated by model 2 is more obvious than the new model. This is due to the fact that in the new model, the slope variation is considered. Initially, due to the higher temperature at the middle point the middle area deforms faster than the surrounding area. As the strain rate and the strain increase in the middle area, both the strain hardening and the strain rate sensitivity increase according to the new model, therefore the middle part needs higher stress to deform. This stress may be even higher than the stress which is necessary for the surrounding area to be deformed. Therefore the deformation of the middle point is delayed, and the strain localization obtained using the new model is not as serious as that obtained using model 2.

6. Conclusions

Tensile material tests have been conducted for the ABS material under the conditions that thermoforming process is performed. Based on the test data, a new model, which could consider the strain hardening, strain rate sensitivity, temperature change, and variation in the hardening index, is proposed. It is proved that the results of this model are in excellent agreement with the uniaxial tensile test result. Compared with the existing material models, the improvement in this new model is clarified.

Acknowledgements

We would like to express our sincere thanks to Denki Kagaku Kogyo Co. Ltd. for providing the test material, and to Mr. H. Kubo for help with some of the experiments.

References

1. H. F. NIED, C. A. TAYLOR and H. G. DELORENZI, *J. Polym. Eng. Sci.* **30** (1990) 1314.
2. W. N. SONG, F. A. MIRZA and J. VLACHOPOULOS, *J. Rheol* **35** (1991) 93.
3. A. RODRIGUEZ-VILLA, J. F. AGASSANT and M. BELLET, Proceedings of the Numerical Methods in Industrial Forming Processes, Numiform'95, Ithaca, N.Y., USA (A. A. Balkema, Rotterdam, 1995) p. 1053.
4. F. M. SCHMIDT, J. F. AGASSANT, M. BELLET and L. DESOUTTER, *J. Non-Newtonian Fluid Mech.* **64** (1996) 19.
5. M. H. VANTAL, B. MONASSE and M. BELLET, Proceedings of the Numerical Methods in Industrial Forming Processes, Numiform'95, Ithaca, N.Y., USA, (A. A. Balkema, Rotterdam, 1995) p. 1089.
6. S. WANG, A. MAKINOUCHI and T. NAKAGAWA, JSPP Symposium96, (Japan Society of Plastic Processing, 1996) p. 149 (In Japanese).
7. *Idem., Advances in Polymer Technology* **17** (1998) 189.
8. J. MEISSNER and J. HOSETTLER, *J. Rheol. Acta* **33** (1994) 1.
9. C. G'SELL and J. J. JONAS, *J. Mater. Sci.* **14** (1979) 583.
10. C. G'SELL, N. A. ALY-HELAL and J. J. JONAS, *ibid.* **18** (1983) 1731.

Received 17 June 1998
and accepted 5 May 1999